J Solid State Electrochem (2008) 12:95–101
DOI 10.1007/s10008-007-0362-9

ORIGINAL PAPER

Characterisation of electroplated $Bi_2(Te_{1-x}Se_x)_3$ alloys

S. Michel · S. Diliberto · N. Stein · B. Bolle · C. Boulanger

Received: 23 February 2007 / Revised: 10 May 2007 / Accepted: 22 May 2007 / Published online: 21 June 2007

Abstract Composition modulated $Bi_2(Te_{1-x}Se_x)_3$ thin films were prepared on stainless steel substrates by cathodic electrodeposition. The composition was dependent on the deposition conditions. It was possible to obtain, in the same electrolyte, films with either an excess or a deficiency of bismuth in relation to stoichiometric $Bi_2(Te_{0.9}Se_{0.1})_3$ by changing the deposition potential or the applied current density. The excess of bismuth was reached at the highest cathodic conditions. The variation of the crystallographic axis and the morphology with a granular structure were correlated with the presence of the Bi enrichment in the ternary. The crystallographic texture of bismuth telluride films was studied according to the electrodeposition conditions. The films presented a fibre texture, and a main orientation {11.0} was observed. Electrical and thermoelectric properties of a $Bi_{1.98}Te_{2.67}Se_{0.39}$ film were measured and showed an *n*-type behaviour.

Keywords Electrochemical growth · Bismuth compounds · Semiconducting materials · Ternary bismuth telluride alloys · Crystallographic texture

S. Michel · S. Diliberto (✉) · N. Stein · C. Boulanger
Laboratoire d'Electrochimie des Matériaux-UMR CNRS 7555,
Université Paul Verlaine-Metz,
1 bd Arago, CP 87811,
57078 Metz cedex 03, France
e-mail: sebastien.diliberto@univ-metz.fr

B. Bolle
Laboratoire d'Etude des Textures et Applications aux Matériaux,
UMR CNRS 7078, Université Paul Verlaine-Metz,
Metz, France

Introduction

Bismuth telluride alloys have a relevant importance for modern solid state technology, owing to their peculiar properties, such as thermoelectric power conversion. These properties have made Bi_2Te_3-based compounds suitable for a large range of applications, such as thermoelectric generators [1], coolers [2] and optical storage systems [3]. Owing to their high figure-of-merit at room temperature, the derivative selenide compounds are considered to be the best *n*-type materials for use in thermoelectric refrigeration at room temperature [4]. Single crystals are usually fabricated by directional crystallisation techniques, while films are obtained by chemical or physical vapour deposition. These deposition techniques have the drawback of a rather high production cost. On the other hand, bismuth telluride alloy electroplating appears to be a promising and low-cost growth method for obtaining films of high quality. Several electrochemical processes have been developed, leading to different compositions of Bi_2Te_3 binary compounds [5–11]. However, there are few studies concerning the Bi-Se-Te ternary [12–14]. In our previous work [13] we used an experimental design to define the chemical and potentiostatic conditions [deposition potential=−55 mV per saturated calomel electrode (SCE)] leading to $Bi_2Te_{2.7}Se_{0.3}$ stoichiometry. The investigations described in this paper are based on this previous work. The electroplating of Bi-Te-Se ternaries was conducted using an electrolyte in the same proportions ($10^{-2} M\ Bi^{3+} + 6\,10^{-3}\ M\ HTeO_2^+ + 6.65\,10^{-4} M\ H_2SeO_3$ and 2 10^{-2} M Bi^{3+} + 1.2 10^{-2} M $HTeO_2^+$ + 1.23 10^{-3} M H_2SeO_3, which correspond, in both cases, to 60 % Bi^{3+}+36% $HTeO_2^+$ + 4% H_2SeO_3 in solution). The aim of this study was to investigate the dependence of phase composition, crystallographic data, surface morphology and crystallographic texture in electro-

plated ternary films on the electrochemical conditions (applied potential or current density).

Experimental procedures

Deposition conditions

Electrolytes were prepared in solution with deionised water. To ensure the stability and the solubility of Bi^{III} solutions, the selected electrolyte was 1 M aqueous HNO_3. The Bi^{III} and Se^{IV} solutions were obtained by dissolution of Bi $(NO_3)_3$,$5H_2O$ and Na_2SeO_3 (analytical grade). The Te^{IV} solutions were prepared from the reaction of nitric acid (2N) on elemental tellurium. Two electrolytes having the same proportions of elements (60% Bi^{3+}+36% $HTeO_2^+ + 4\%$ H_2SeO_3 in solution) were used to obtain ternary films: 10^{-2} M Bi^{3+}+6 10^{-3} M $HTeO_2^+ + 6.65\ 10^{-4}$ M H_2SeO_3 and 2 10^{-2} M Bi^{3+}+1.2 10^{-2} M $HTeO_2^+ + 1.23\ 10^{-3}$ M H_2SeO_3.

Stainless-steel discs were chosen as substrate for the preparation of $Bi_2(Te_xSe_{1-x})_3$ films. The plates were mechanically polished with SiC paper and with diamond paste (1 μm size). After being polished, the electrodes were cleaned with distilled water followed by rinsing with p.a. grade methanol. The working electrodes were located horizontally in the bottom of a PTFE cell specially designed in our laboratory. An area of 2 cm^2 was exposed for deposition. The deposition, using a potentiostat/galvanostat Radiometer PGP 201 driven by a computer, was carried out at room temperature without stirring with a platinum disc counter electrode facing the working plate and with a saturated calomel electrode (SCE). The growth time was fixed at 2 h. Deposition was conducted either at potentiostatic polarisations ranging from −55 mV/SCE to −125 mV/SCE or at cathodic current densities ranging from −0.07 A.dm^{-2} to −0.40 A.dm^{-2}. The electrochemical cell had an electrolyte volume of 0.1 dm^3. The electrolyte solution was de-aerated by argon bubbling through it for 20 min prior to the experiment, and this atmosphere was then kept constant.

Deposit characterisation

Samples were prepared after electrodeposition by being thoroughly rinsed in three steps (nitric acid solution, pH=1, deionised water, and methanol), followed by air drying. The morphology was studied under a scanning electron microscope (Hitachi model S 2500LB or Philips model XL 30). X-ray diffraction data were obtained with an Inel diffractometer (curve detector INEL CPS 120, CoK_α radiation). The crystallographic texture was determined by X-ray diffraction pole figure measurement using FeK_α radiation. The goniometer was equipped with a curve sensitive detector INEL CPS 120 having a 120° angular aperture and configured to record simultaneously several pole figures and their background. This method is called multi-pole figure measurement. Although $Bi_2(Te_{1-x}Se_x)_3$ presents a rhombohedral structure, a pseudo-hexagonal cell was used [15]. Thus, all the crystallographic notations are given according to the notation used for the hexagonal structure (four indices notation). The {01.5}, {10.10}, {11.0} and {20.5} pole figures were measured on the deposits removed from their substrate. These planes were chosen because of their relatively high intensities. All the measurements were corrected from background.

Elemental analyses were carried out using an electron probe microanalyser (CAMECA SX 50) that had been calibrated with Bi_2Te_3 and Bi_2Se_3 standards. The tellurium, bismuth and selenium microanalyses were performed on ten different sections of the samples. The stoichiometry was assessed using the average of these ten values and assuming an atomic composition of 5 in the sample. Analyses were reproducible within ± 1 atomic percentage (at%).

The electronic and transport properties of the electrodeposited $Bi_xTe_ySe_z$ materials were determined by measurement of the Seebeck coefficient, the electrical resistivity and the carrier concentration. The sample was removed from the substrate with an epoxy resin to ensure the integrity of the film. The Seebeck coefficient was measured, at room temperature, using a Keithley 2700 multimeter. The voltage was measured between two probes, which were held at a fixed distance of 2 cm from each other. The hot probe was heated to a temperature 2 °C higher than the other one. Electrical resistivity and carrier concentration were determined by the Van Der Pauw technique and Hall method, respectively, with a HEM-2000 EGK system.

Results and discussion

Two alternative types (potentiostatic and galvanostatic) of electroplating were explored in two electrolytes containing 60% Bi^{3+}, 36% $HTeO_2^+$, 4% H_2SeO_3 with [Bi^3+]=10^{-2} M or 2 10^{-2} M.

Chemical composition analyses

Figure 1 shows the variations in the Bi, Se and Te percentages as a function of deposition potential and electrolyte composition. For the [Bi^{3+}]=0.01 M, as the potential decreases, the tellurium and selenium contents in the electrodeposits continuously decrease, while a concomitant increase in the percentage of bismuth is observed. For a solution having the same Bi/Se/Te proportions but twice as concentrated, the behaviour is different. For the potential ranging between −55 mV and −90 mV, the stoichiometry

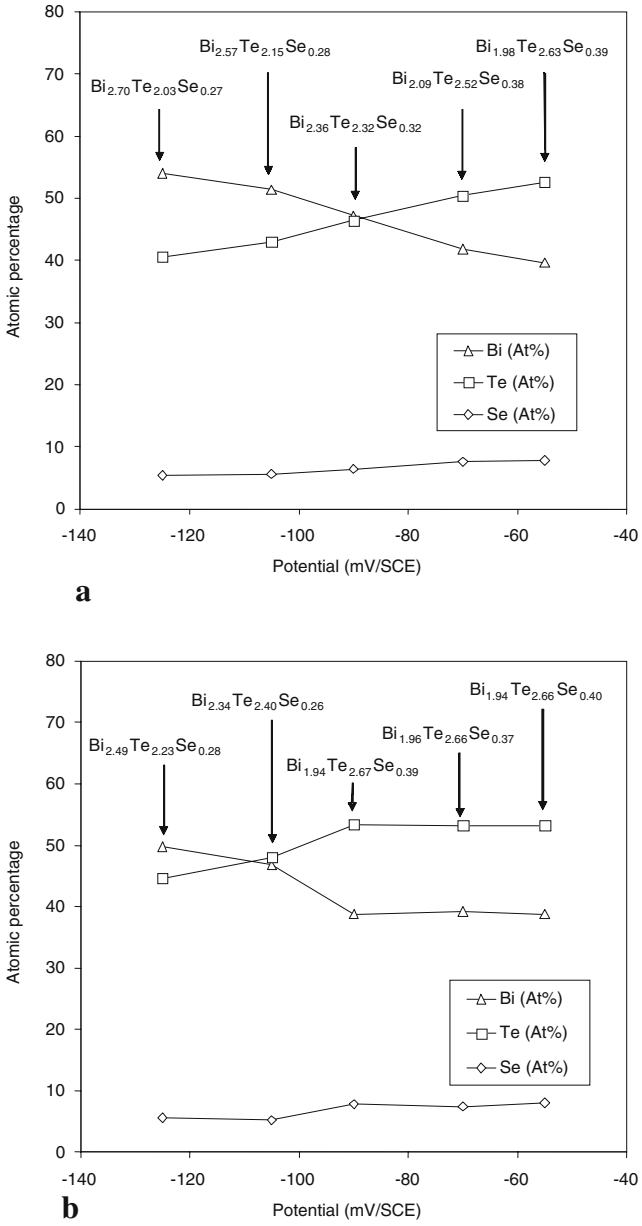

Fig. 1 Evolution of Bi, Te and Se atomic percentages in films vs the deposition potential and the bismuth concentration in the electrolyte containing 60% Bi^{3+}, 36% $HTeO_2^+$, 4% H_2SeO_3 with $[Bi^{3+}]=10^{-2}$ M (**a**) or 2.10^{-2} M (**b**). (*The ternary stoichiometry is also indicated*)

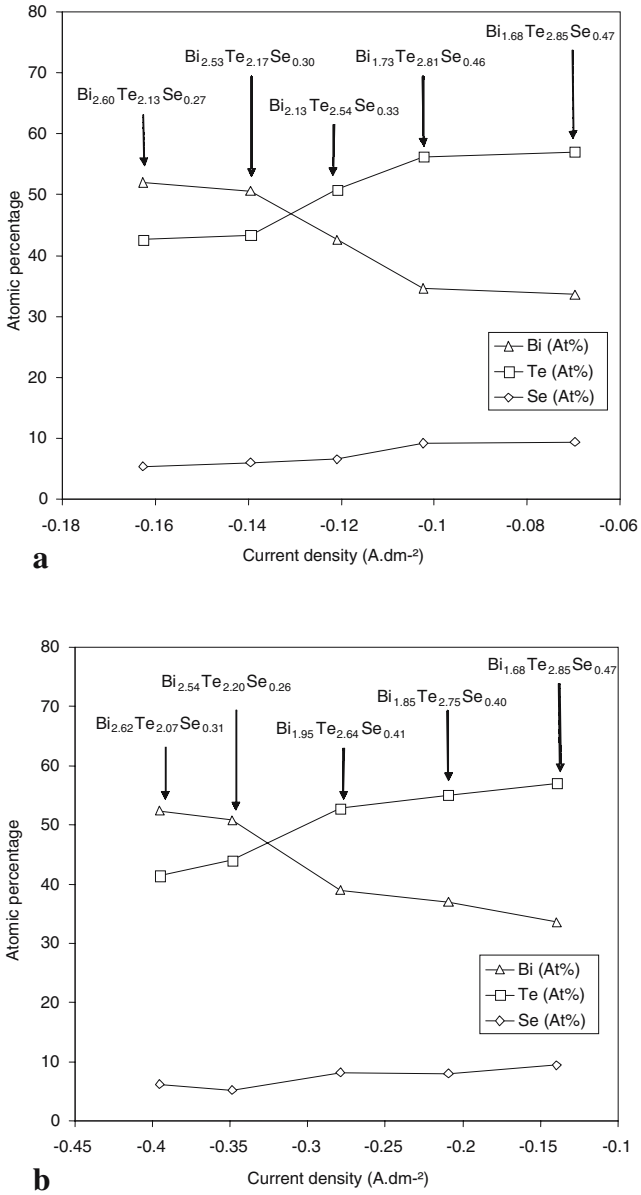

Fig. 2 Evolution of Bi, Te and Se atomic percentages in films vs the current density and the bismuth concentration in the electrolyte containing 60% Bi^{3+}, 36% $HTeO_2^+$, 4% H_2SeO_3 with $[Bi^{3+}]=10^{-2}$ M (**a**) or 2.10^{-2} M (**b**). (*The ternary stoichiometry is also indicated*)

remained stable. Higher cathodic potentials caused a rapid increase of bismuth, an important decrease of tellurium and a small fall of selenium content in the films. The current density dependence of film composition is plotted in Fig. 2. The curves have the same shape whatever the electrolyte concentration, but, for the twice-as-concentrated solution, $Bi_2Te_{2.7}Se_{0.3}$ type compounds are obtained at higher cathodic current densities. The same variation in the element content can be noted as that observed in the potentiostatic plating with a bismuth concentration of 0.02 M.

By controlling the electrode potential or the current densities, it was possible to achieve a large range of ternary film compositions. Higher cathodic conditions caused bismuth enrichment, while lower cathodic conditions led to chalcogenide (X=Se+Te)-rich alloys. This variation is similar to that in our previous study relative to the electroplating of bismuth telluride binary [10]. Decreasing the potential resulted in increased deposition of Bi. The explanation reported by Gonzales et al. [9] is that the reduction potential of Bi^{3+} is slightly more negative than that of Bi_2Te_3 or, in our case, the Bi-Se-Te ternary. The experimental values leading to a transition between Bi-rich

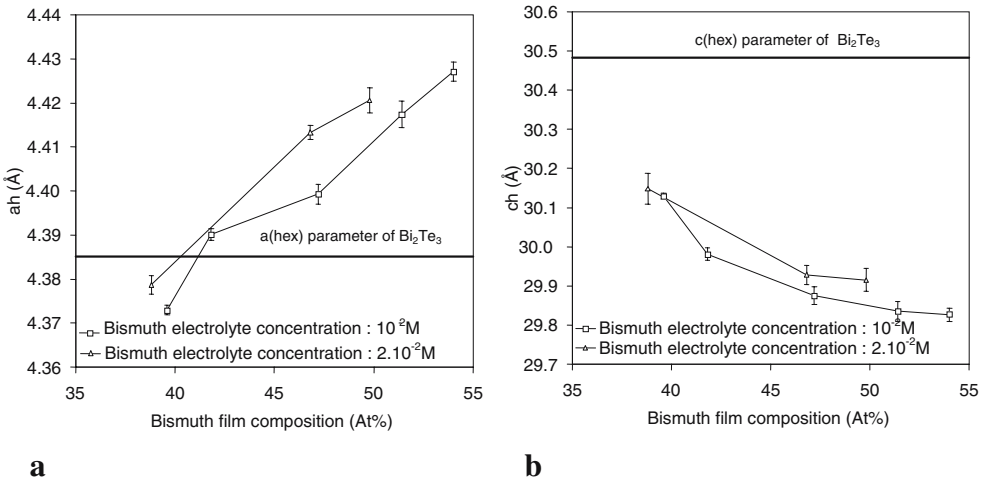

Fig. 3 Hexagonal a_{hex} (**a**) and c_{hex} (**b**) lattice parameters vs the amount of bismuth in the electrolytes of the potentiostatic electrodeposited films containing 60% Bi^{3+}, 36% $HTeO_2^+$, 4% H_2SeO_3 with $[Bi^{3+}]=10^{-2}$ M or 2.10^{-2} M

and X-rich ternary films were, for the potentiostatic plating, $E_{deposition}$ equal to −55 mV for $[Bi^{3+}]=0.01$ M and −90 mV for $[Bi^{3+}]=0.02$ M, and, for the galvanostatic plating, a current density equal to −0.11 A/dm^2 for $[Bi^{3+}]=0.01$ M and −0.30 A/dm^2 for $[Bi^{3+}]=0.02$ M. A similar trend was observed in the case of the binary electroplating.

The growth rate varies between 3 μm h^{-1} (for $|Bi^{3+}|=10^{-2}$ M and E=−55 mV) and 6 μm h^{-1} (for |Bi|=2 10^{-2} M and E=−105 mV) for potentiostatic plating. The galvanostatic growth rates were found to range between 3 μm h^{-1} and 10 μm h^{-1}, according to the experimental conditions. The electroplating efficiencies were close to 98±2% and

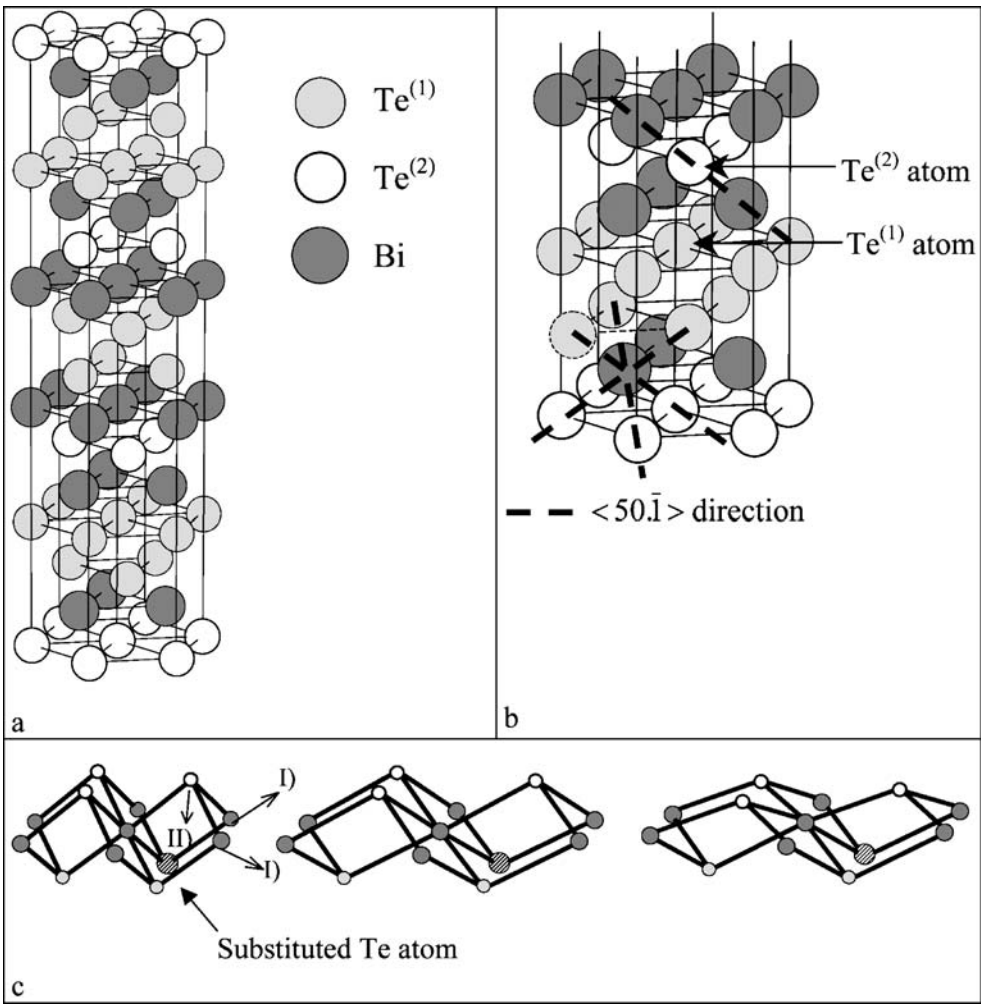

Fig. 4 Crystallographic structure of Bi_2Te_3. **a** Stacking of hexagonal net of Bi and Te atoms. **b** Enlargement of the structure. *The dotted lines* correspond to the dense directions. **c** Evolution of the distance between atoms when a Te atom is substituted by a Bi atom

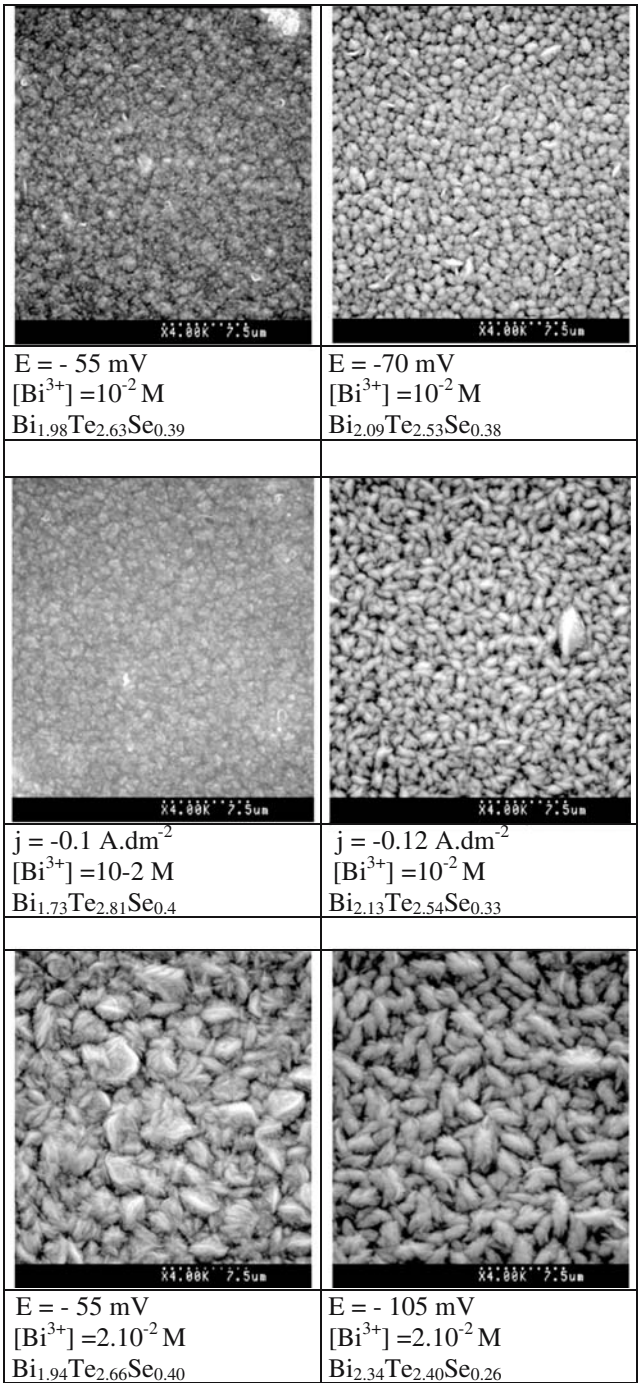

E = - 55 mV $[Bi^{3+}] = 10^{-2}$ M $Bi_{1.98}Te_{2.63}Se_{0.39}$	E = -70 mV $[Bi^{3+}] = 10^{-2}$ M $Bi_{2.09}Te_{2.53}Se_{0.38}$
j = -0.1 A.dm^{-2} $[Bi^{3+}]$ =10-2 M $Bi_{1.73}Te_{2.81}Se_{0.4}$	j = -0.12 A.dm^{-2} $[Bi^{3+}] = 10^{-2}$ M $Bi_{2.13}Te_{2.54}Se_{0.33}$
E = - 55 mV $[Bi^{3+}] = 2.10^{-2}$ M $Bi_{1.94}Te_{2.66}Se_{0.40}$	E = - 105 mV $[Bi^{3+}] = 2.10^{-2}$ M $Bi_{2.34}Te_{2.40}Se_{0.26}$

Fig. 5 SEM photographs of electrodeposited films obtained by a potentiostatic or galvanostatic mode in an electrolyte containing 60% Bi^{3+}, 36% $HTeO_2^+$, 4% H_2SeO_3

did not change significantly with electrolyte concentration, $E_{deposition}$, or current density.

X-ray diffraction study

X-ray diffraction (XRD) was employed to control the structure of films deposited at various potentials and current densities. For all samples, the diffraction peaks were indexed according to the crystallographic structure of Bi_2Te_3 but with a small shift in lattice parameters. Examination of the diffraction patterns revealed that the electrodeposits were not formed from the separate elements but corresponded to a single phase closer to Bi_2Te_3 than to Bi_2Se_3.

The lattice parameters of the hexagonal structure for all electrodeposits were determined from the observed reticular distances, using a least-squares method. Figure 3 shows the relationship between the refined lattice parameters of the films and the bismuth atomic percentage for potentiostatic deposits. It can be noticed that, for the sample with 40 at% Bi, a_{hex} and c_{hex} are lower than the Bi_2te_3 cell parameters (Fig. 3a and b). This is probably due to the presence of a small quantity of Se and its lower atomic radius. Nevertheless, the Se quantity did not change with the cathodic potential or intensity; consequently, the cell parameters can be exclusively expressed according to the Bi stoichiometry. As for the Bi_2Te_3 compounds [8, 10], when the cathodic potential is increased, so increasing the amount of bismuth, the a_{hex} parameter (Fig. 3a) increases while the c_{hex} parameter decreases (Fig. 3b). The same general observations were noted for the a-axis and c-axis lengths of galvanostatic deposits.

To understand these variations, one must remember the particular crystallographic structure of $Bi_2(Te_{0.9}Se_{0.1})_3$, which can be described with the Bi_2Te_3 structure, where some Te atoms are statistically replaced by Se atoms. The Bi_2Te_3 structure is formed by a layered periodic arrangement of atoms. In a layer the atoms form a hexagonal net. These layers were aligned perpendicularly to the trigonal c axis in a stacking ABCABC..., characteristic of a face-centred cubic crystal. The change in atomic species and spacing distinguishes this structure from fcc. The layers of atoms could get together to form a quintet composed of five atomic planes arranged according to the following pattern: $Te^{(1)}$-Bi-$Te^{(2)}$-Bi-$Te^{(1)}$. In the quintet, the Bi-$Te^{(1)}$ and Bi-$Te^{(2)}$ bonds are mainly covalent and the quintets are bonded by Van der Waals interactions. According to the atomic positions of Bi and Te given by Wyckoff [16] Fig. 4a shows the structure of Bi_2Te_3. In the basal plane (hexagonal net) of the structure, the distance between neighbouring atoms (equal to the a_{hex} lattice parameter) is larger than the atomic size of the atoms. Crystallographic analysis shows that the shorter distances between neighbouring atoms (covalent bonds Bi-$Te^{(2)}$ and Bi-$Te^{(1)}$) are close to the same directions and are along the $\langle 50.\bar{1} \rangle$ directions (dotted line in Fig. 4b). Therefore, in a quintet along one of these dense directions the pattern is only described by the covalent bonds.

If the the atomic radii of Bi (1.54 Å), Te (1.43 Å) and Se (1.16 Å) are taken into account, the replacement of a Te or an Se atom by a Bi atom increases the distance between the substituted Te atom and the neighbouring atoms along the

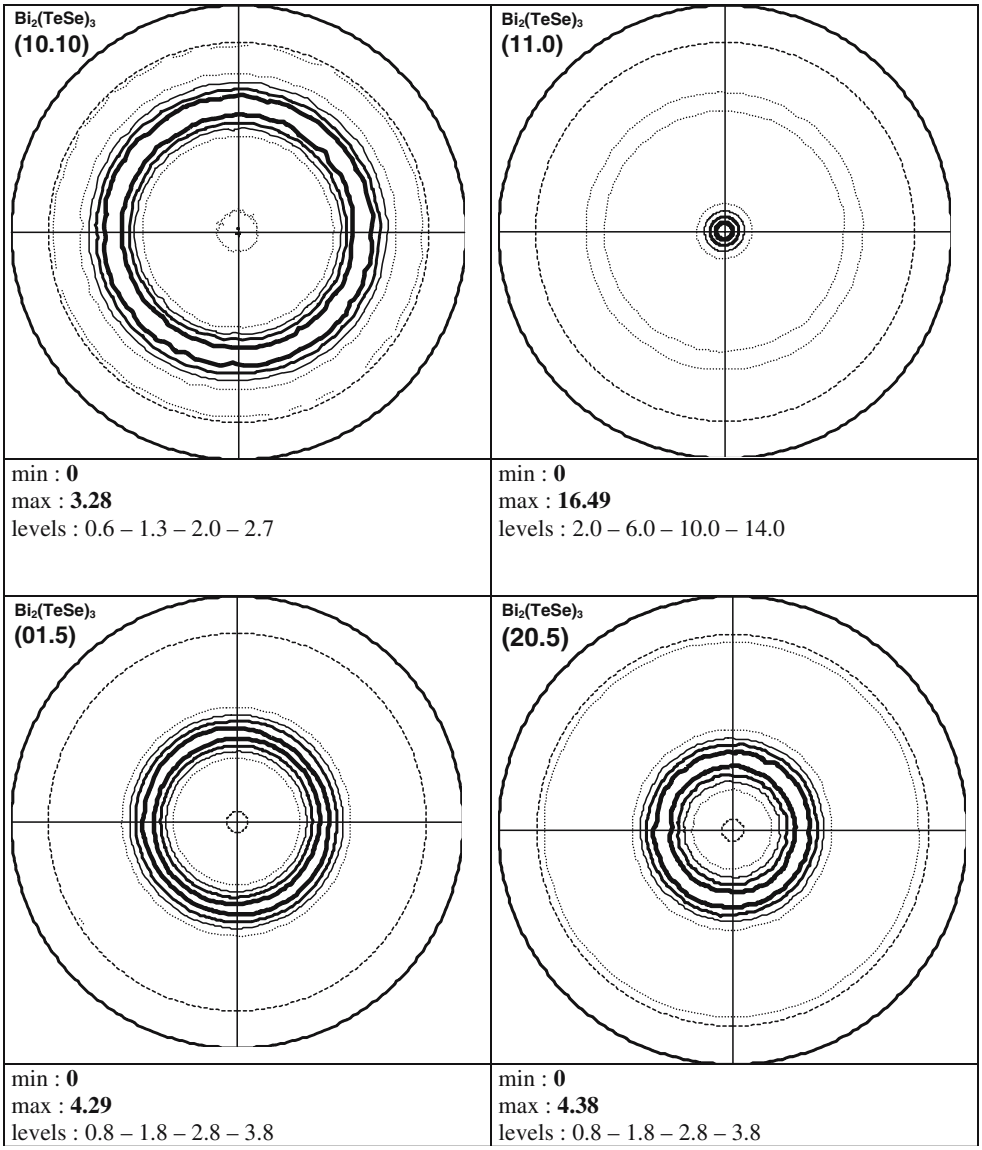

Fig. 6 Radial pole figure (intensity integrated along azimuth angle in multiple of random unit versus tilt angle) of the $Bi_2(TeSe)_3$ films obtained with deposition potentials equal to −90 mV/SCE, electrolyte: 10^{-2} M Bi^{3+}+6.10^{-3} M $HTeO_2^+$+$6.65.10^{-4}$ M H_2SeO_3

dense direction. The substitution of a Te atom (marked by an arrow in Fig. 4b) induces a modification in the position of the Bi atoms in the next plane. This leads to an increase in the distance between these Bi atoms in the stacking plane (a_{hex} lattice parameter) and to an increase in the distance between the plane containing the substituted atoms and the next Bi planes. As the distance between the atoms in the basal plane increases, the distance between the Bi and the Te non-substituted planes decreases, leading to a decrease in the c_{hex} lattice parameter. These modifications are summarised in Fig. 4c.

Characterisation by scanning electron microscope

Scanning electron microscope (SEM) images present the surface morphology of ternary samples with equivalent compositions and elaborated under potentiostatic and galvanostatic conditions (Fig. 5). The figure evidences that potentiostatic films are totally covered by a large number of agglomerated nodules, in contrast to the binary, where the surfaces are covered by agglomerated needles. The size of nodules depends on the synthesis conditions and the stoichiometric composition. For films presenting a chalcogen excess (Fig. 5a and c) obtained from an electrolyte with $[Bi^{3+}]$=0.01 M, a little roughness and a fine granular microstructure were observed, whereas the Bi-rich ternary films presented a larger granular structure (Fig. 5b and d). The electrochemical mode did not seem to induce an important difference for the morphology, even if the smallest nodules were obtained in the galvanostatic mode. The morphology was rather fixed by the film stoichiometry. For $[Bi^{3+}]$=0.02 M (Fig. 5e and f), the films presented a granular structure, whatever the composition. The deposit structure was coarser, with larger nodules.

Characterisation of crystallographic texture

The effect of the potential deposition or current density on the crystallographic texture of the electrodeposit was also investigated. The deposition was carried out for the two electrolyte concentrations. The films presented a fibre texture with the normal direction of the deposit as fibre axis. The {01.5}, {10.10}, {11.0} and {20.5} pole figures were measured on samples obtained for −70 mV/SCE with $[Bi^{3+}]$=0.01 M (Fig. 6). Similar results were found for potentiostatic or galvanostatic depositions. A single preferred orientation {11.0} was always observed for deposits obtained with an electrolyte having a $|Bi^{3+}|$ concentration of 0.01 M, whatever the electroplating mode. This orientation was also mainly obtained for depositions obtained with electrolyte having a $[Bi^{3+}]$ concentration of 0.02 M. Nevertheless, for the most cathodic potential (E=−125 mV), the dominant {11.0} orientation was still observed, but a concomitant {10.10} preferential orientation appeared. This texture and its evolution with the stoichiometry were similar to that already studied in our previous work on bismuth telluride [17]. The substitution of tellurium atoms by selenium atoms in the crystallographic structure did not change the film growth mechanism. The orientation {11.0} was the main one observed. This {11.0} orientation indicates that the crystallites of the deposits are such that the basal planes are perpendicular to the electrode surface, with the position of the c axis parallel to the surface. This orientation is favourable to the transfer of electrons from the electrode and thus to the electrochemical process.

Electrical and Seebeck characterisation

Some electrical measurements were made at room temperature directly on five films with a composition equal to that of $Bi_{1.98}Te_{2.67}Se_{0.39}$, corresponding to the best stoichiometry for thermoelectric applications. The carrier concentration reached 4.5 10^{20} cm^{-3}, the electron mobility was 10.8 $cm^2V^{-1}s^{-1}$. The observed values of Seebeck coefficients and the Hall effect were all negative, and these results indicate that all samples exhibited *n*-type features, with similar values of approximately −70 μV K^{-1} except for one, a Seebeck coefficient equal to−150 μV K^{-1}. Although the electrodeposited ternary has levels of carrier concentration similar to those of bulk material, the Seebeck coefficients, as well as the Hall mobility, are lower than that in a single crystal, respectively around −240 μV K^{-1} and 45 $cm^2V^{-1}s^{-1}$. This can be due to the microstructure of the films. Defaults and cracks, and grain boundaries in the films probably caused the strong decrease of electron mobility and Seebeck coefficient. A more detailed study of the thermoelectric properties of electrodeposited $Bi_2(Te_{1-x}Se_x)_3$ films has been submitted [18].

Conclusion

$Bi_2(TeSe)_3$ films were obtained by potentiostatic and galvanostatic electrodeposition. The composition of the films was studied as a function of the deposition potential and of the current density. The films had a wide range of compositions accessible by electrochemical deposition, showing the possibility of the preparation of Bi-rich or Te-rich $Bi_2(Te_{0.9}Se_{0.1})_3$. All samples were single phase and polycrystalline. The morphology of the alloy deposits was not directly influenced by the electrochemical condition but, on the whole, by their chemical composition. Electrodeposition always led to a preferential orientation. {11.0} is the dominant orientation, corresponding to the presence of the basal planes perpendicular to the electrode surface. Bismuth seleno-telluride showed a semi-conducting nature, with *n*-type electrical conductivity.

References

1. Rowe DM, Bhandari CM (1983) Modern thermoelectrics. Reston Publishing, London
2. Goldsmid HJ, Douglas RW (1954) J Appl Phys 5:386
3. Lou DY (1982) Appl Opt 21:1602
4. Nolas GS, Sharp J, Goldsmid HJ (2001) Thermoelectrics basic principles and new materials developments. Springer, Berlin Heidelberg New York
5. Takahashi M, Katou Y, Nagata K, Furuta S (1994) Thin Solid Films 240:70
6. Magri P, Boulanger C, Lecuire JM (1996) J Mater Chem 6:773
7. Fleurial JP, Borshcheevsky A, Ryan MA, Phillips WM, Snyder JG, Caillat T, Kolawa EA, Herman JA, Mueller P, Nicolet N (1999) Mater Res Soc 545:493
8. Miyazaki Y, Kajitani T (2001) J Cryst Growth 229:542
9. Martin-Gonzales M, Prieto AL, Gronsky R, Sands T, Stacy AM (2001) J Electrochem Soc 149:C546
10. Michel S, Diliberto S, Boulanger C, Stein N, Lecuire JM (2005) J Cryst Growth 277:274
11. Tittes K, Bund A, Plieth W, Bentien A, Paschen S, Plöttner M, Gräfe H, Fischer WJ (2003) J Solid State Electrochem 7:714
12. Fleurial JP, Ryan MA, Borshcheevsky A, Phillips WM, Kolawa EA, Snyder JG, Caillat T, Kaschich T, Mueller P (2000) Microfabricated thermoelectric power generation devices, patent no WO 00/08693
13. Michel S, Stein N, Schneider M, Boulanger C, Lecuire JM (2003) J Appl Electrochem 33:23
14. Bu L, Wang W, Wang H (2007) Appl Surf Sci 253:3360
15. Powder Diffraction File, Joint Committee on Powder Diffraction Standards, no 15–863
16. Wyckoff RWG (1964) Crystal Structures. Wiley, New York
17. Michel S, Diliberto S, Boulanger C, Bolle B (2006) J Cryst Growth 296:227
18. Zimmer A, Stein N, Terryn H, Boulanger C (2007) J Phys Chem Solids (in press). DOI 10.1016/j.jpcs.2007.05.021